# Dissolution kinetics of aluminosilicates from biomass ashes in alkaline solutions

Küçük Mehmet Emin, Kinnarinen Teemu, Häkkinen Antti



**DOI:** 10.1016/j.ceramint.2021.01.011

Ceramics International xxx (xxxx) xxx

Contents lists available at ScienceDirect

Ceramics International

journal homepage: www.elsevier.com/locate/ceramint

# Dissolution kinetics of aluminosilicates from biomass ashes in alkaline solutions

Mehmet Emin Küçük *, Teemu Kinnarinen, Antti Häkkinen

*Lappeenranta-Lahti University of Technology, School of Engineering Science, Yliopistonkatu 34, 53850 Lappeenranta, Finland*

ARTICLE INFO

*Keywords:*
Biomass fly ash
Aluminosilicates
Dissolution
Geopolymer

ABSTRACT

This research explores the influence of fly ash source, alkali concentration and temperature on the dissolution kinetics of Al and Si. The characteristics of the reaction products and the solid residue were evaluated with ICP-MS, SEM-EDS, and quantitative XRD. It was found that Al dissolution occurs faster with a higher yield compared to Si for both ash types. The temperature and the NaOH concentration had a similar effect on the dissolution of Al, while the dissolution of Si was influenced more by the NaOH concentration. The simultaneous dissolution of aluminosilicates was achieved by keeping the temperature at 30 °C, where the precipitation of Al was prevented, and the concentration of the dissolved Si was close to its maximum value. The Kabai Model was the most suitable to explain the dissolution of Al for both ash sources, while the Si dissolution was described with 1-dimensional diffusion, Jander and Ginstling-Brounsthein models.

## 1. Introduction

With an amount of 4.1 million tonnes annually, cement production is one of the largest industries in the world [1]. However, for each metric tonne of cement produced, approximately 750 kg of $CO_2$ is released to the atmosphere; therefore, the cement industry is responsible for 7% of total anthropogenic $CO_2$ emissions globally [2]. According to the 2030 climate & energy framework adopted by the European Council in October 2014, the target for 2030 is to reduce GHG emissions by 40% (from 1990 levels), by increasing the share of renewable energy to at least 32% [3].

For the reduction of $CO_2$ emissions resulting from the construction industry, a great number of studies have been conducted focusing on cement replacement materials [4,5]. One group of these materials, geopolymer composites, can be utilised in the construction industry as alternative construction materials because of their good durability [6,7], mechanical properties [8,9], microstructural characteristics [8], and workability [9]. A geopolymer is an amorphous to semi-crystalline three-dimensional material formed by the polymerisation of alumino-silicate compounds under alkaline conditions (e.g., NaOH or KOH) and ambient temperatures [10]. Previous research has established that the geopolymerisation process involves three stages: (1) the dissolution and hydrolysis of the amorphous Al and Si from the source material in an alkaline solution; (2) the transportation of the dissolved ions into monomers (precipitation and gelation); and (3) the poly-condensation of the precipitated nuclei for the formation of the 3-D network of poly (sialate), poly (sialate-siloxo) or poly (sialate-disiloxo) structures [11].

The properties of the final geopolymer composite are strongly affected by the concentration [6] and type of the alkaline source; the properties and composition of the aluminosilicate source [8]; the particle size distribution of the raw materials [8]; the curing temperature and curing time [6]; the solution to solid ratio [12]; and the ratio of Si to Al and $Na_2SiO_3$ to NaOH [13–15]. Therefore, it is possible to optimise the geopolymerisation process and improve the properties of the final geopolymer composite by enhancing the release rates of Al and Si in the dissolution reaction. The reactions taking place at the abovementioned stage (1) can be described as follows:

$$Al_2O_3 + 3H_2O + 2OH^- \rightarrow 2Al(OH)_4^- \quad (1)$$

$$SiO_2 + H_2O + 2OH^- \rightarrow [SiO(OH)]^- \quad (2)$$

$$SiO_2 + 2OH^- \rightarrow [SiO_2(OH)_2]^{2-} \quad (3)$$

The availability of aluminosilicates in raw materials has a substantial influence on the final properties of the geopolymer composites. Several materials with high contents of Al and Si have been investigated as aluminosilicate sources, including fly ash [13,16], ground granulated blast furnace slag (GGBFS) [15] and metakaolin [17]. Due to its

* Corresponding author.
*E-mail address:* mehmet.kucuk@lut.fi (M.E. Küçük).

https://doi.org/10.1016/j.ceramint.2021.01.011
Received 23 October 2020; Received in revised form 13 December 2020; Accepted 4 January 2021
Available online 6 January 2021

**Table 1**
Experimental parameters used in the study for the investigation of biomass fly ash dissolution in NaOH solutions.

| Experiment | NaOH concentration, (M) | Sampling time, (h) | Temperature, (°C) |
|---|---|---|---|
| 1 | 3 | 1.5, 3, 6, 12, 24, 72 | 60 |
| | 6 | 1.5, 3, 6, 12, 24, 72 | 60 |
| | 9 | 1.5, 3, 6, 12, 24, 72 | 60 |
| | 12 | 1, 1.5, 2, 3, 6, 12, 24, 72 | 60 |
| | 15 | 1.5, 3, 6, 12, 24, 72 | 60 |
| 2 | 12 | 1, 1.5, 2, 3, 6, 12, 24, 72, 120, 168, 216 | 20 |
| | 12 | 1, 1.5, 2, 3, 6, 12, 24, 72, 120, 168, 216 | 30 |
| | 12 | 1, 1.5, 2, 3, 6, 12, 24, 72, 120 | 40 |

**Table 2**
Rate equations applicable to dissolution reactions [24,25,27].

| Name | Type | Equation | Number |
|---|---|---|---|
| Exponential law | A | $kt = ln\alpha$ | 1 |
| Power law | A | $kt = \alpha^{1/n}$ | 2 |
| 1D diffusion | D | $kt = \alpha^2$ | 3 |
| 2D diffusion for cylinder (Valensi) | D | $kt = (1-\alpha)\ln(1-\alpha) + \alpha$ | 4 |
| 3D diffusion for sphere (Jander) | D | $kt = \left[1-(1-\alpha)^{1/3}\right]^2$ | 5 |
| 3D diffusion for sphere (Ginstling-Brounsthein) | D | $kt = \left(1-\frac{2\alpha}{3}\right) - (1-\alpha)^{2/3}$ | 6 |
| First order | D | $kt = -\ln(1-\alpha)$ | 7 |
| Second order | D | $kt = (1-\alpha)^{-1}$ | 8 |
| Modified first order (Kabai) | V | $alnk + alnt = lnln(1/(1-\alpha))$ | 9 |
| Contracting volume (Shrinking core) | D | $kt = 1-(1-\alpha)^{1/3}$ | 10 |
| Contraction area (Shrinking disc) | D | $kt = 1-(1-\alpha)^{1/2}$ | 11 |
| Random nucleation 2D diffusion (Avrami-Erofejev) | S | $kt = [-\ln(1-\alpha)]^{1/2}$ | 12 |
| Random nucleation 3D diffusion (Avrami-Erofejev) | S | $kt = [-\ln(1-\alpha)]^{1/3}$ | 13 |
| Prout - Tompkins | S | $kt = \ln[\alpha/(1-\alpha)]$ | 14 |

k: reaction rate constant ($s^{-1}$), t: time (s), α: reaction extent, a: constant of average order, A: acceleratory, D: deceleratory, S: sigmoidal, V: variable.

favourable chemical composition, particle characteristics and low cost, fly ash has been frequently applied as an aluminosilicate source. However, the determination of the reactive Si and Al in fly ash is of challenging scientific and technical interest. Despite its high aluminosilicate content, the heterogeneous structure of fly ash limits the dissolution of Al and Si into the alkaline media [16,19]. Between the two phases that compose fly ash, the reactive part is present in the vitreous phase, while the crystalline phase is comprised of quartz, which has a significantly higher activation energy for silica hydrolysis compared to that in the vitreous phase [18,19].

Several authors have examined the effects of different parameters on the dissolution characteristics of fly ash. Cristelo et al. [16] studied the influence of temperature and mechanical activation on the dissolution reaction for a local Class F fly ash. Their results demonstrate that the time required to solve the same amount of bulk mass from fly ash can be reduced from 90 days to 1 day by increasing the temperature from 20 to 80 °C, indicating the significant effect of temperature on the reaction kinetics. Additionally, the temperature increase had a considerable effect on the equilibrium concentrations. Finally, they observed that the Avrami model could satisfactorily describe the dissolution kinetics. In a comprehensive study by Kuenzel and Ranjbar [20], investigating the effects of different parameters on the dissolution reaction of class F fly

**Table 3**
EDS and XRF results of biomass-based fly ashes, values expressed in wt.%.

| EDS | | | XRF | | |
|---|---|---|---|---|---|
| Element | FA1 | FA2 | Component | FA1 | FA2 |
| Al | 6.4 ± 0.3 | 3.3 ± 0.2 | $Al_2O_3$ | 17.69 ± 0.15 | 11.08 ± 0.15 |
| Si | 5.9 ± 0.1 | 5.7 ± 0.4 | $SiO_2$ | 24.41 ± 0.47 | 27.72 ± 0.47 |
| Ca | 31.1 ± 0.1 | 27.3 ± 0.6 | CaO | 34.67 ± 0.28 | 31.49 ± 0.28 |
| Fe | 0.8 ± 0.1 | 1.8 ± 0.2 | $Fe_2O_3$ | 1.66 ± 0.21 | 4.55 ± 0.21 |
| S | 2.9 ± 0.1 | 6.6 ± 0.1 | $SO_3$ | 4.30 ± 0.11 | 6.26 ± 0.11 |
| Mg | 1.1 ± 0.2 | 1.3 | MgO | 2.91 ± 0.22 | 3.45 ± 0.22 |
| K | 3.3 ± 0.2 | 3.2 ± 0.1 | $K_2O$ | 3.00 ± 0.05 | 2.27 ± 0.05 |
| Na | 1.7 | 3.6 ± 0.1 | $Na_2O$ | 2.00 ± 0.07 | 2.77 ± 0.07 |
| P | 1.1 | 0.7 | $P_2O_5$ | 2.29 ± 0.06 | 1.63 ± 0.06 |
| Mn | 1.3 | 0.6 | $Mn_3O_4$ | 1.13 ± 0.11 | 0.66 ± 0.01 |
| Ti | 0.2 | 1.4 | $TiO_2$ | 0.25 ± 0.02 | 1.94 ± 0.02 |
| Zn | – | 1.2 | ZnO | 0.28 ± 0.01 | 0.47 ± 0.01 |
| Cl | 1.0 | 3.5 ± 0.1 | BaO | 0.18 | 0.36 |
| O | 36.2 ± 0.2 | 35.2 ± 0.3 | CuO | 0.01 | 0.23 |
| C | 6.9 ± 0.3 | 4.5 ± 0.2 | $Cr_2O_3$ | 0.03 ± 0.01 | 0.09 ± 0.01 |
| | | | $LOI_{950°C}$ | 5.0 | 4.8 |

ash, both temperature and time showed a stronger impact on the dissolution of Al and Si than the concentration of the alkaline solution. It was also demonstrated that at least 8 M of NaOH solution should be utilised for the determination of the reactive fraction of fly ash. This limitation was attributed to the heterogeneous structure of fly ash which contains a partially reactive fraction in addition to the inert and reactive phases, whose dissolution is significantly affected by the dissolution conditions. In another study [21], the influence of the reaction time, and the type and concentration of the alkaline solutions on the dissolution of various aluminosilicate sources were examined including coal fly ash, kaolin, metakaolin, pozzolana, slag, and zeolite. Dissolution percentage of 20% for Al and Si was achieved for fly ash in 24 h in 10 M NaOH solution. Furthermore, it was reported that the dissolution of Al and Si may have followed a similar path as the Si/Al ratio was constant throughout the dissolution. A recent study [19] focused on the determination of the potential reactivity of class F fly ash for geopolymerisation with a two-step sequential leaching process (NaOH and HCl). It was discovered that the reactive Al and Si fraction is significantly different from the total amounts of these elements present in fly ash; therefore, it was suggested that the reactive Si/Al ratios should be used instead of the total or glassy phases [19]. In a study investigating the dissolution of aluminosilicates from two different types of biomass ash, Chaunsali et al. [22] found that the dissolution degrees of Al and Si in 2 M NaOH solution were measured as 20% and 45% for Silverton ash, and as 15% and 35% for Bindless ash after 7 days. The differences in the dissolved concentrations for different ash types were attributed to the amorphous content. Another study [23] that examined the dissolution of Si from a silicious biomass ash reported that up to 68% of the total Si was dissolved in 1 M NaOH after 28 days. The dissolution degree of Si declined to 30% in presence of additional $Ca(OH)_2$ due to the formation of C–S–H gel.

In contrast to coal fly ash, there is much less information about the effects of reaction conditions on the dissolution of biomass-based fly ash. Distinctly different chemical characteristics of biomass-based ashes compared to coal-based fly ash [5] can affect the dissolution of aluminosilicates significantly. Previously published studies have tended to examine dissolution of pre-treated ashes [16,29] in mildly alkaline environments [22,23,29], while this paper attempts to show the dissolution behaviour of different biomass ashes without any pre-treatment in a comparative perspective at a wide range of alkalinity, temperature, and reaction time. The primary aim of this study is to systematically investigate the effects of ash source, dissolution time, concentration of the alkaline solution, and temperature on the dissolution of different

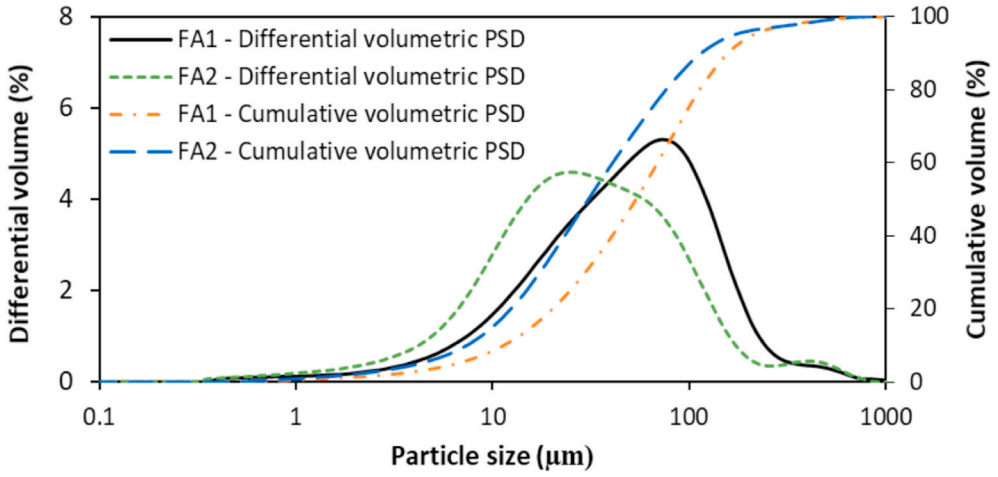


**Fig. 1.** Particle size distributions of the biomass fly ashes.

biomass ashes from different origins. Additionally, the kinetics of the dissolution reaction were investigated using different reaction rate models. This study makes a major contribution to advancing an understanding on the suitability of biomass-based fly ashes as raw materials for geopolymer composites.

## 2. Materials and methods

### 2.1. Materials and methods

The biomass-based ash samples were provided by local Finnish kraft pulp mills using bark, wood residues, paper mill reject sludge, and wastewater sludge. Biomass fly ash 1 (FA1) was collected from a bark boiler unit of a pulp mill that uses bark, wood residues and paper mill reject sludge as fuel in Southeast, Finland. Biomass fly ash 2 (FA2) was supplied from a co-incineration plant of a paper mill located in Southeast Finland with bark, wood chips, recycled wood, natural gas, and wastewater sludge as fuels. Sodium hydroxide solutions were prepared by dissolving NaOH pellets with 99% purity in deionised water. The solutions were allowed to cool down at room temperature prior to their use in the dissolution experiments.

A laser diffraction particle size analyser with a Hydro EV dispersing unit was utilised for the PSD measurements of the initial fly ash samples with Fraunhofer calculation model (Malvern Mastersizer 3000, Malvern Instruments, UK). The dissolution tests were performed in a shaker (Heidolph, Unimax 1010, Germany), with a heating unit (Heidolph, Inkubator 1000, Germany). Sample surface morphologies were investigated with a scanning electron microscope (Hitachi SU 3500 scanning electron microscope, Japan), and an energy-dispersive X-ray spectroscopy (EDS) mapping was used to obtain the elemental compositions of the samples (Thermo Scientific, Ultra dry SDD detectors, USA) by using Pathfilder Software. The presented EDS results represent averages of three measurements. A BET specific surface analyser was utilised for the quantification of the specific surface areas of the ashes (Micromeritics 3Flex). The elemental compositions were obtained with a sequential X-Ray fluorescence (XRF) spectrophotometer (Bruker AXS S4 Pioneer, USA). The ash samples were crushed and prepared according to the glass fusion technique. The concentrations were determined by comparing the results of measurements with known standards. The Wroxi method, developed by PanAlytical and validated by using international Certified Reference Materials (CRM), was utilised in the XRF study. The mineral compositions of the samples were investigated by X-ray diffraction (XRD) analysis (Bruker D8 Advance X-ray diffractometer, Cu source – $K\alpha = 1.5406$ Å, $2\theta = 10–70^{\circ}$ range with $0.02^{\circ}$ steps, 0.7 step/sec., sample rotation of 15 rpm, divergence slit of $0.3^{\circ}$) after they were ground in an agate mortar. A Rietveld analysis was performed to the XRD data by using a TOPAS Software, and rutile was applied as the internal standard for obtaining quantitative estimates of the sample compositions. An inductively coupled plasma-mass spectrometry (ICP-MS) was used for the determination of the metal concentrations in the dry samples after their complete dissolution by using standardised 4-acid digestion and peroxide smelt digestion methods.

### 2.2. Experimental

The ashes were dried in an electrical oven at 105 °C for 24 h for moisture removal and they were then homogenised to obtain a more uniform composition for the dissolution experiments. The dissolution tests were conducted for solutions containing 4 g of solid and 40 g of NaOH solution (liquid/solid ratio of 10) in a 60 mL reactor for certain hours under continuous shaking. The influence of NaOH molarity, temperature, and reaction time on the dissolution of aluminium and silicon was investigated for two types of biomass fly ash from different origins. The dissolution results presented in the study are averages of two different dissolution experiments. The experimental design is illustrated in Table 1, and the experimental procedure was identical for both samples.

Concentrations of dissolved Al and Si in the NaOH solutions were determined by an Agilent 7900 inductively coupled plasma mass spectrometer. The filtration of the clear supernatant was performed by using a syringe filter (Phenex RC 0.45 µm) prior to the ICP-MS analysis. Since the solutions were highly concentrated with respect to Al and Si, and ICP-MS gives the most accurate results for the concentrations below 100 ppb [19], the samples were diluted 1000 times prior to the analysis.

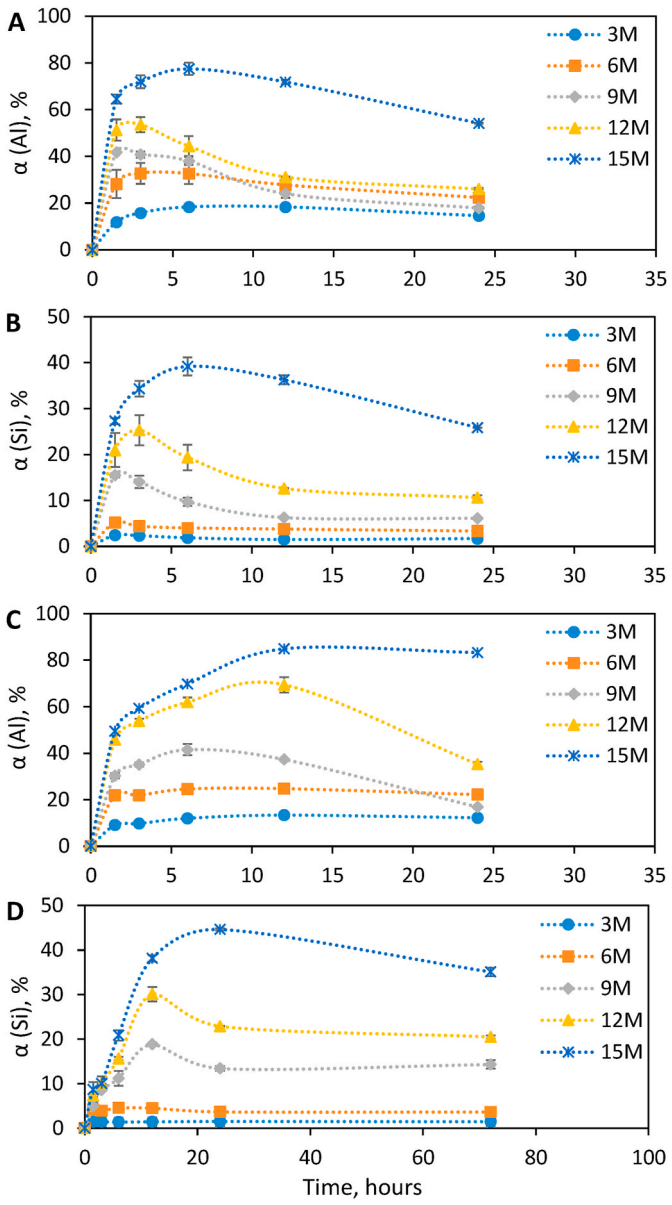


**Fig. 2.** Effect of NaOH concentration on Al (A) and Si (B) dissolution for FA1, and on Al (C) and Si (D) for FA2 at 60 °C. *α*: dissolved mass of Al or Si/total mass of Al or Si in dry solid.

Calibration solutions with the concentrations of 10 ppb, 25 ppb, 40 ppb, 50 ppb, 100 ppb, 200 ppb and 400 ppb were utilised to verify the accuracy of the results. Following the filtration step, the solid residues were washed with distilled water (wash ratio > 50) for the removal of free NaOH, before the XRD and SEM/EDS analysis.

### 2.3. Modelling

The dissolution of biomass fly ash with NaOH solution is a heterogeneous solid-liquid reaction where the solid particles are surrounded by liquid. Based on the shape of the reaction isotherms and the reaction mechanism, various reaction rate models [24,25] have been developed to investigate heterogeneous solid-liquid reactions [16,26]. Table 2 presents fourteen rate models that have been studied in this paper. The suitability of the kinetic models has been evaluated on the basis of coefficients of determination ($R^2$).

Both Exponential law (1) and Power law (2) have acceleratory t - α curves. 1 dimensional diffusion (1DD, 3), Valensi (4), Jander (5), and Ginstling-Brounsthein (6) models describe a diffusion-controlled reaction, where the rate determining step is the diffusion of either the reactant(s), or the reaction product(s) to or from the boundary layer [24, 26]. First order (7) and second order (8) models have a deceleratory t - α curve. First order rate model (7) is not capable of representing the early stages of a reaction with an induction period. Both models (7 and 8) well define reactions with a high initial reaction rate because α decreases as the reaction proceeds [27]. The Kabai model [25] was derived from the Nernst equation by describing the reaction rate constant k from an experimentally derived expression K ($\alpha/(t^{1-a})$). Kabai [25] then verified his experimentally obtained expression by comparing the combined fundamental rate expression with a mathematical equation. In the Kabai model, the kinetic curve is determined by *a*, which depicts a constant of an average order. For $a > 1$, the kinetic curve is sigmoidal and acceleratory in its first part, and it is deceleratory for $a < 1$. It describes a surface-reaction controlled solid-liquid heterogeneous reaction [25,26]. Shrinking core (10) and shrinking disc models (11) are geometric models with a deceleratory t - α curve. In shrinking core model (10), the rate law is derived for spherical particles where the volume of the solid decreases as the reaction proceeds. Shrinking disc model (11) considers a cylindrical rod whose length remains the same, but its area decreases during the reaction [27]. Avrami-Erofejev rate laws (12 and 13) have a sigmoidal t - α curve, and they indicate a nucleation-controlled reaction for a cylindrical (12) and cubical or spherical (13) reactive particles. 2D diffusion model (12) gives a straight line in the t – $[\ln (1-\alpha)]^{1/n}$ graph, while it is concave downward in case of 3D diffusion model [27]. Prout-Tompkins equation (14) has a sigmoidal t - α curve, and it is applied to investigate the kinetics of reactions which can be terminated once the product is formed [27].

## 3. Results and discussion

### 3.1. Characteristics of the biomass ashes

The chemical compositions of the biomass fly ash samples obtained by EDS and XRF are shown in Table 3. The analysis results show high concentrations of CaO, followed by $SiO_2$ and $Al_2O_3$, which have also been reported in other studies [5,28]. The total amount of Al and Si in dry solids were quantified with ICP-MS analysis, and Al and Si concentrations were measured as 98 600 and 123 000 mg/kg dry solid in FA1, while they were measured as 57 800 and 127 000 mg/kg dry solid in FA2. The comparison of the different analysis methods is not straightforward as EDS and ICP give the results as actual element compositions, whereas the concentrations are expressed as oxides in the case of XRF. Furthermore, EDS and XRF are solid state analysis techniques different from ICP, which is performed in liquid phase after complete dissolution of samples.

The particle size distributions of the fly ashes are presented in Fig. 1. D10, D50 and D90 values were measured as 11.3, 53.7, and 358 μm for FA1; and 7.32, 30.7, and 116 μm for FA2. The BET specific surface areas (SSA) of the fly ashes were quantified as 9.27 and 1.73 $m^2/g$. The significantly higher SSA of FA1 compared to that of FA2 may be due to its large number of porous particles, which can also enhance the dissolution reaction by creating more active sites for mass transfer.

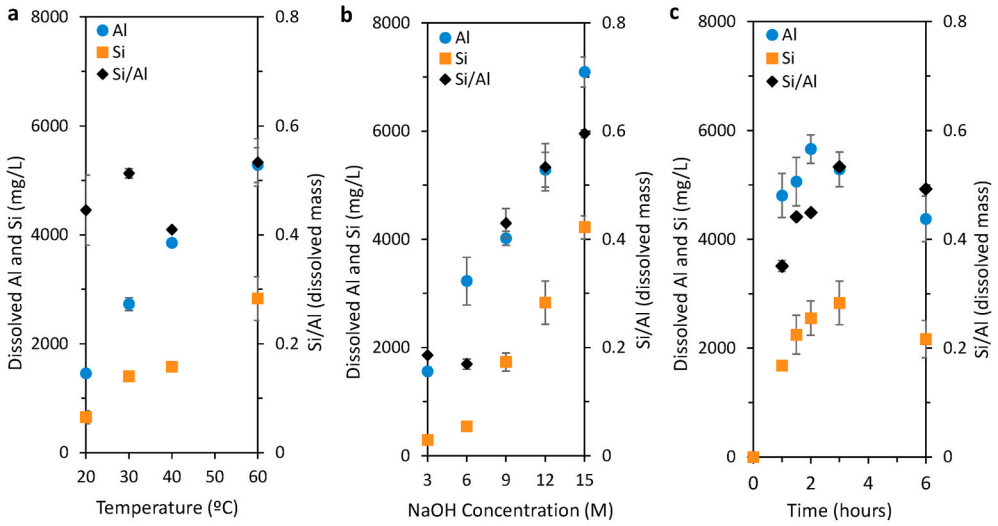


**Fig. 3.** ICP results for dissolved Al and Si from FA1 as a function of a) temperature, b) NaOH concentration, and c) time. Unless otherwise specified, the dissolution duration, NaOH concentration, and temperature were 3 h, 12 M, and 60 °C, respectively.

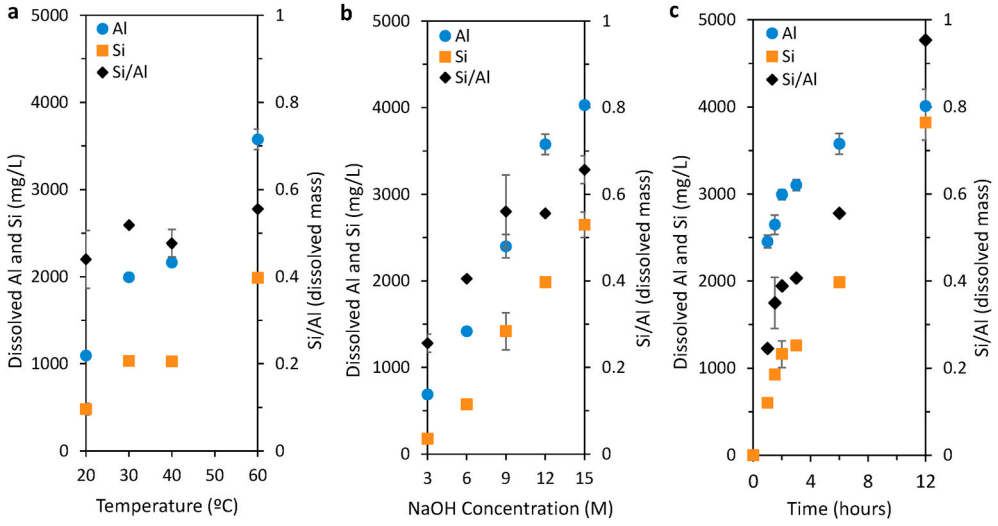


**Fig. 4.** ICP results for dissolved Al and Si from FA2 as a function of a) temperature, b) NaOH concentration, and c) time. Unless otherwise specified, the dissolution duration, NaOH concentration, and temperature were 6 h, 12 M, and 60 °C, respectively.

### *3.2. Influence of NaOH concentration*

Fig. 2 presents the influence of NaOH concentration on the dissolution of Al and Si from the biomass ash samples at a constant temperature of 60 °C. The dissolved fractions (%) were calculated as the ratio of the total mass of the element in the solution to the total mass present in dry solids, which were measured with the ICP-MS. For both types of biomass fly ash, the maximum dissolved concentrations were obtained at a NaOH concentration of 15 M (Fig. 2). The positive correlation between the solubility of Al and Si, and the NaOH concentration finds support from previous studies [16,17,21,23,29,31]. Nikolić et al. [31] demonstrated that when the NaOH concentration was increased from 5 M to 10 M, the dissolved fraction of Al increased from 6% to 19%, and the dissolved fraction of Si increased from 4% to 7% in 2 h. The dissolved fractions of Al and Si increase over time until the maximum concentration points, after which their concentrations start to decrease due to gelation/precipitation. During the initial dissolution stage, the Si–O–Si, Al–O–Al and Si–O–Al bonds are broken into silicate and aluminate monomers due to the attack of $OH^-$ which subsequently form the $[SiO(OH)_3]^-$, $[SiO_2(OH)_2]^{2-}$, and $[Al(OH)_4]^-$ forms. The positive correlation

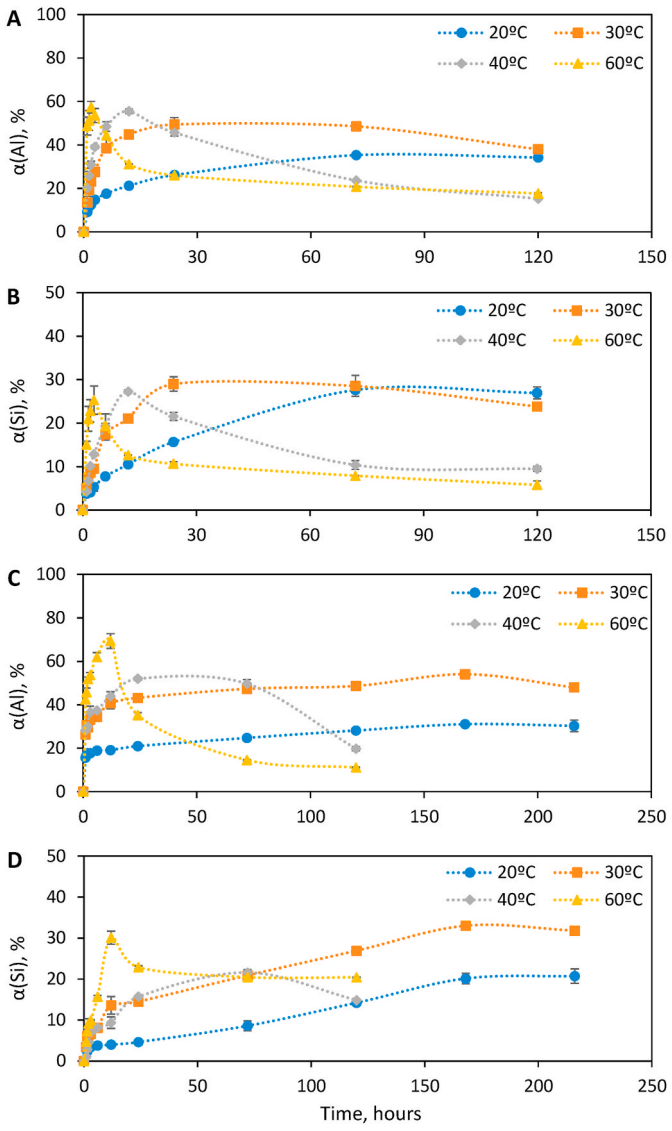


**Fig. 5.** Effect of temperature on Al (A) and Si (B) dissolution for FA1, and on Al (C) and Si (D) for FA2 at 12 M NaOH. *α*: dissolved mass of Al or Si/total mass of Al or Si in dry solid.

between the solution alkalinity and the concentrations of dissolved Al and Si may be explained by the strong influence of the solution pH on the dissolution of aluminosilicates. It is considered [30] that the rate-determining step during the Si dissolution is the breakage of neutral or negatively charged surface siloxane bonds (>$Si_2O$) which subsequently are transformed into the silanol species by the attack of $OH^-$ and $H_2O$. In the case of highly alkaline systems, the water molecules attack the surface siloxane groups next to the negatively charged silanol groups (>$SiO^-$ or $SiO^-M^+$), eventually enhancing the Si dissolution with an increasing pH.

By keeping the dissolution temperature (60 °C) and the duration (3 h for FA1, and 12 h for FA2) constant, the Si/Al ratios increase for both samples (Fig. 3b and Fig. 4b), which demonstrates that the alkalinity has a greater effect on the dissolution of Si compared to that of Al. Despite this observation, the concentration of dissolved Al is always higher than that of Si for all NaOH concentrations. These results reflect those of Nikolíc et al. [31] who also found that Al dissolution occurred at a higher degree than that of Si in concentrated NaOH solutions. This may be explained by weaker Al–O bonds compared to Si–O bonds [16], and a lower electrical charge imbalance of Si during the dissolution reaction. In highly alkaline solutions, however, the electrically neutral surface of Si becomes more negatively charged due to the increased amount of ≡$SiOH^-$ ionic groups which favours the breakage of Si–O–Si bonds [31]. It is well recognised that the soluble quantities of Al and Si play a crucial role in the determination of the microstructure and mechanical properties of the final geopolymer composite [20,29]. The production of geopolymer composites from the aluminosilicate precursors is dependent on the availability of reactive Al and Si, which also determines the characteristics of the geopolymer gel. In the absence of sufficient alkalinity, the dissolution of Si is hampered by a comparatively rapid Al release and a more crystalline zeolite structure is obtained; however, proper dissolution of Al is necessary for the production of aluminosilicate gel [29,33].

The maximum dissolved concentrations in the current study were measured approximately as 80% and 40% for Al and Si in 15 M NaOH at 60 °C, respectively. These results agree with the maximum concentrations of 20% and 50% reported by Chaunsali et al. [22] for Al and Si from Silverton ash, 16% and 42% for Al and Si from Bindless (biomass) fly ash and a NaOH concentration of 2 M at ambient temperature. Similarly, the highest dissolution percentages reported for Al and Si in electric arc furnace steel slag were 34% and 25% in 10 M NaOH at 60 °C, respectively [31]. Finally, a dissolution degree of 20% was achieved for both Al and Si in 10 M NaOH at room temperature [21], and of 35% for Si from silicious biomass fly ash in 1 M NaOH after 200 h [23].

### 3.3. *Influence of temperature*

The effect of temperature on the dissolution of biomass fly ashes was investigated at 20, 30, 40 and 60 °C by using a NaOH concentration of 12 M. As presented in Fig. 5, an increase in the temperature accelerated the dissolution of both Al and Si from the samples. With an increase in temperature, both Al and Si dissolved faster; thus, the saturation points were reached sooner, and the dissolved concentrations started to decline earlier due to precipitation, which is in accordance with earlier findings by Granizo et al. [17]. In addition to the effect of temperature on the dissolution kinetics, Fig. 5. (A and C) shows that there was a slight rise in the maximum dissolved Al concentrations with the temperature. The maximum concentrations of Al were achieved at 60 °C for both FA1 and FA2, which was followed by the concentrations obtained at 40, 30, and 20 °C, respectively. The maximum degree of the Al dissolution from FA1 was observed to increase from 35% to 58%, and from 32% to 69% from FA2 when temperature increased from 20 to 60 °C. The maximum concentrations of Si showed no variance with increasing temperature in the case of FA1, whereas in the case of FA2 it increased from 21% to 30% at 20 °C and at 60 °C, respectively. It can thus be suggested that 60 °C

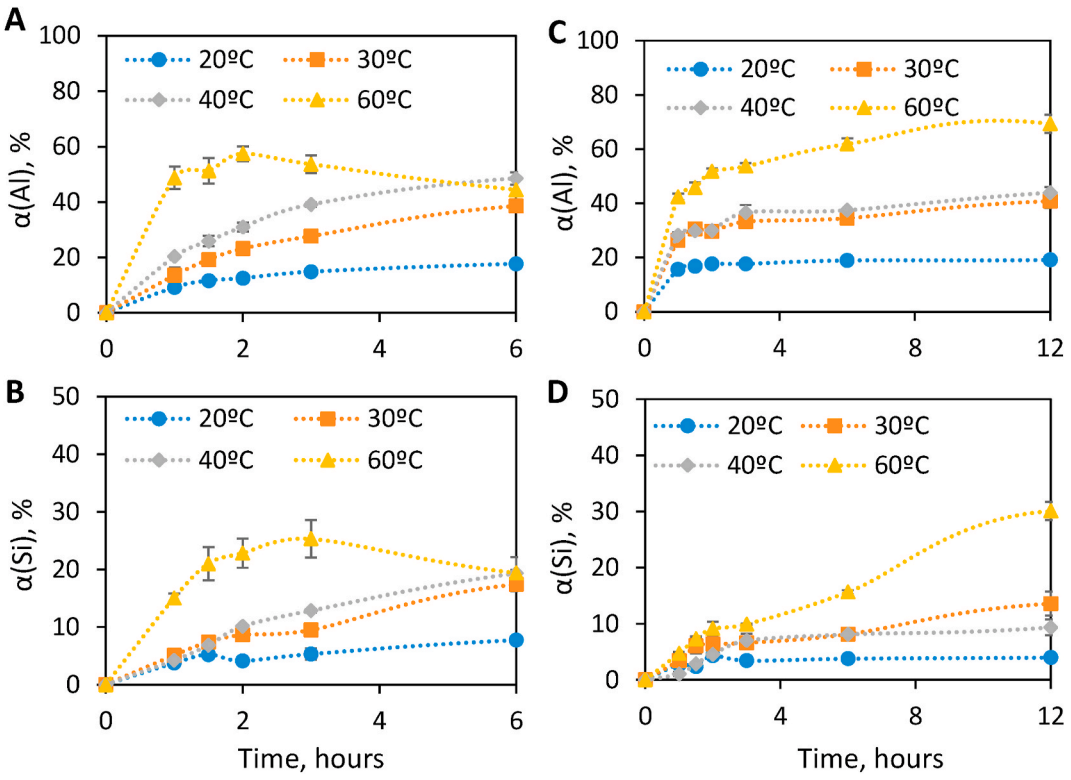


**Fig. 6.** Effect of temperature on Al (A) and Si (B) dissolution for FA1, and on Al (C) and Si (D) for FA2 at 12 M NaOH in the early stages of dissolution. $\alpha$: dissolved mass of Al or Si/total mass of Al or Si in dry solid.

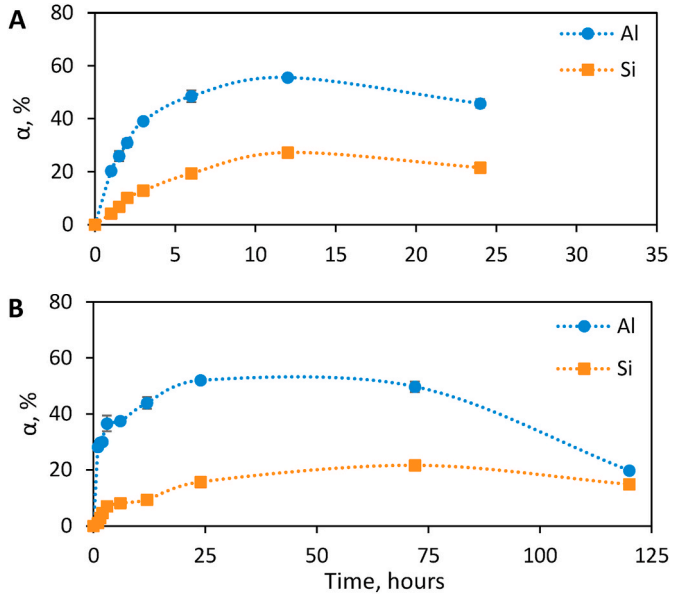


**Fig. 7.** Dissolution of Al and Si in FA1 (A) and FA2 (B) in 12 M NaOH at 40 °C as a function of time, $\alpha$: dissolved mass of Al or Si/total mass of Al or Si in dry solid.

and higher temperatures may be required to increase the Si dissolution from FA2. Such a trend was reported by Kuenzel and Ranjbar [20] who studied the dissolution of fly ash in NaOH-activated geopolymers and found that the dissolution of Si increased substantially when the temperature is higher than 85 °C.

The earlier stages of the dissolution of Al and Si are presented in Fig. 6, which illustrates that the dissolved Si fractions increase proportionally with the increase of temperature. By keeping the temperature at 30 °C, it was possible to optimise the conditions in such a way that, the dissolved Si amount was very close to its maximum value, without the precipitation of Al, which hinders the simultaneous dissolution of aluminosilicates at high temperatures (40 and 60 °C). The dissolution of Al and Si is controlled by the chemical reaction at the surface of the particles, by diffusion through the product layer or through a liquid film, and therefore, a change in temperature changes the diffusion coefficient which subsequently facilitates or hampers the release of aluminosilicates [31]. As illustrated in Fig. 3a-b and Fig. 4a-b, the applied temperature has a smaller influence on the dissolution of Al and Si compared to NaOH concentration. This result is rather contradictory to that of Kuenzel and Ranjbar [20], who observed that temperature (when higher than 85 °C) had a greater effect on aluminosilicates dissolution than the alkalinity of the solution. This difference may be attributed to the lower dissolution temperature applied in the current study. It was previously reported that the temperature increase accelerated the dissolution kinetics of aluminosilicates from co-fired ashes (coal and biomass ash mixture), while a minor increase in the reaction extent was observed when the temperature was increased from 43 to 63 °C [32].

**Table 4**
Dissolution rate parameters for FA1 and FA2 in 12 M NaOH at 40 °C.

| Sample | | | FA1 | | | | FA2 | |
|---|---|---|---|---|---|---|---|---|
| Model | Al | | Si | | Al | | Si | |
| Equation | $R^2$ | $k$, $s^{-1}$ | $R^2$ | $k$, $s^{-1}$ | $R^2$ | $k_{,,}$ $s^{s-1}$ | $R^2$ | $k_{,}$ , $s^{s-1}$ |
| 1 | 0.744 | $2{\cdot}10^{-5}$ | 0.766 | $4{\cdot}10^{-5}$ | 0.911 | $7{\cdot}10^{-6}$ | 0.505 | $8{\cdot}10^{-6}$ |
| 2 | 0.649 | $3{\cdot}10^{-5}$ | 0.723 | $2{\cdot}10^{-5}$ | 0.522 | $1{\cdot}10^{-5}$ | 0.512 | $3{\cdot}10^{-6}$ |
| 3 | 0.942 | $8{\cdot}10^{-6}$ | 0.993 | $2{\cdot}10^{-6}$ | 0.844 | $4{\cdot}10^{-6}$ | 0.972 | $2{\cdot}10^{-7}$ |
| 4 | 0.957 | $5{\cdot}10^{-6}$ | 0.991 | $9{\cdot}10^{-7}$ | 0.872 | $2{\cdot}10^{-6}$ | 0.975 | $1{\cdot}10^{-7}$ |
| 5 | 0.971 | $1{\cdot}10^{-6}$ | 0.989 | $2{\cdot}10^{-7}$ | 0.899 | $6{\cdot}10^{-7}$ | 0.978 | $2{\cdot}10^{-8}$ |
| 6 | 0.962 | $1{\cdot}10^{-6}$ | 0.991 | $2{\cdot}10^{-7}$ | 0.881 | $5{\cdot}10^{-7}$ | 0.976 | $2{\cdot}10^{-8}$ |
| 7 | 0.870 | $2{\cdot}10^{-5}$ | 0.933 | $7{\cdot}10^{-6}$ | 0.726 | $1{\cdot}10^{-5}$ | 0.839 | $1{\cdot}10^{-6}$ |
| 8 | 0.908 | $3{\cdot}10^{-5}$ | 0.889 | $9{\cdot}10^{-6}$ | 0.819 | $2{\cdot}10^{-5}$ | 0.872 | $1{\cdot}10^{-6}$ |
| 9 | 0.971 | $2{\cdot}10^{-5}$ | 0.966 | $6{\cdot}10^{-6}$ | 0.980 | $3{\cdot}10^{-6}$ | 0.878 | $6{\cdot}10^{-7}$ |
| 10 | 0.850 | $7{\cdot}10^{-6}$ | 0.951 | $3{\cdot}10^{-6}$ | 0.704 | $3{\cdot}10^{-6}$ | 0.832 | $4{\cdot}10^{-7}$ |
| 11 | 0.841 | $1{\cdot}10^{-5}$ | 0.949 | $4{\cdot}10^{-6}$ | 0.693 | $5{\cdot}10^{-6}$ | 0.829 | $5{\cdot}10^{-7}$ |
| 12 | 0.735 | $3{\cdot}10^{-5}$ | 0.814 | $2{\cdot}10^{-5}$ | 0.560 | $1{\cdot}10^{-5}$ | 0.623 | $2{\cdot}10^{-6}$ |
| 13 | 0.678 | $3{\cdot}10^{-5}$ | 0.737 | $2{\cdot}10^{-5}$ | 0.543 | $2{\cdot}10^{-5}$ | 0.524 | $3{\cdot}10^{-6}$ |
| 14 | 0.807 | $4{\cdot}10^{-5}$ | 0.799 | $5{\cdot}10^{-5}$ | 0.939 | $1{\cdot}10^{-5}$ | 0.536 | $9{\cdot}10^{-6}$ |

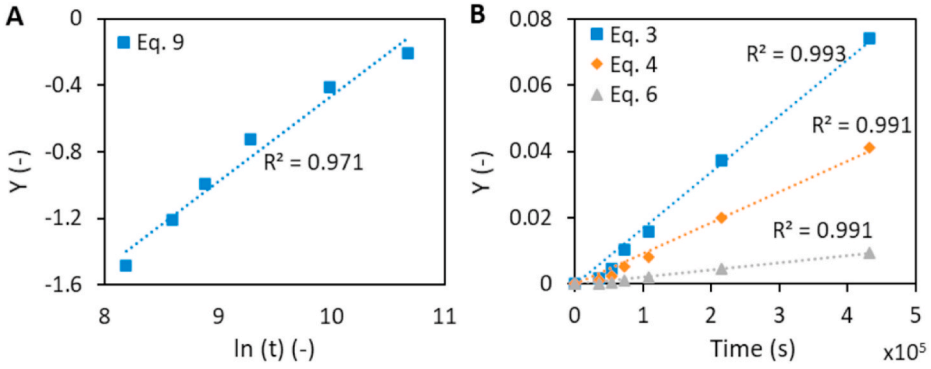


**Fig. 8.** Model fittings of FA1 for dissolution of Al (A) and Si (B), Kabai (Eq. 9), 1D-diffusion (Eq. (3)), Valensi (Eq. 4), and Ginstling– Brounsthein (Eq. 6).

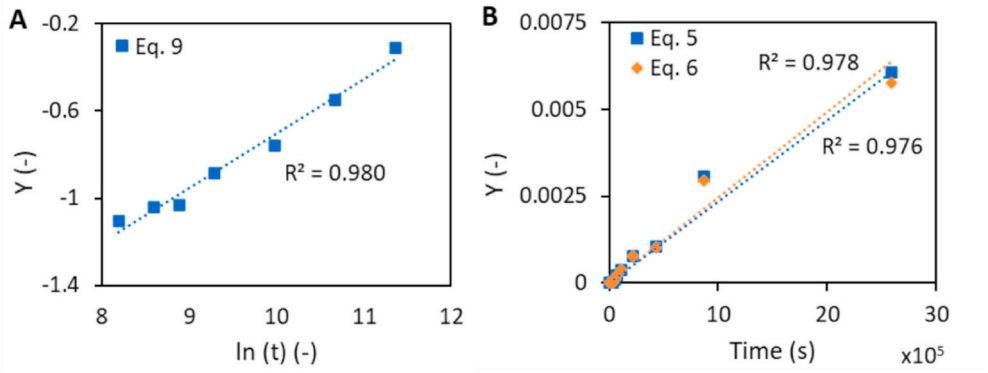


**Fig. 9.** Fitting of Kabai (Eq. 9), Jander (Eq. 5) and Ginstling–Brounsthein (Eq. 6) models for Al (A) and Si (B) from FA2.

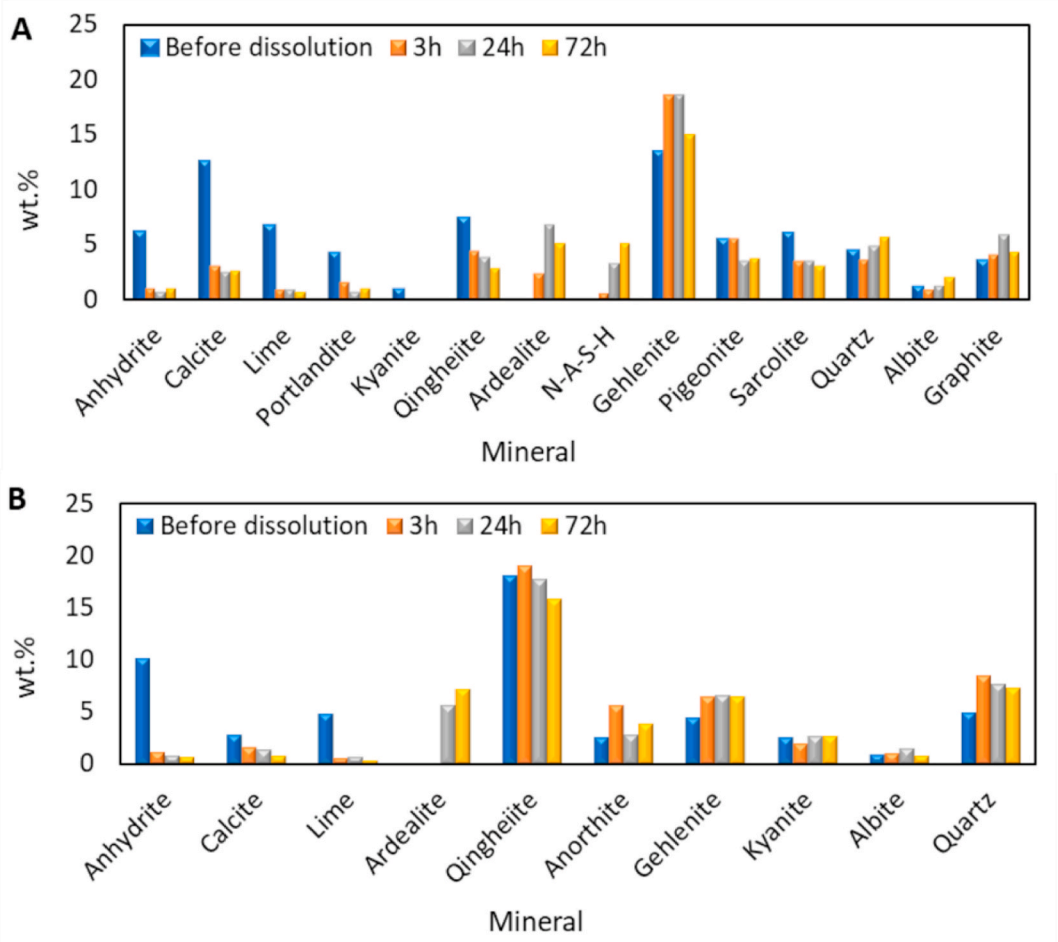


**Fig. 10.** Quantitative XRD results of A: FA1, and B: FA2 with respect to the dissolution time.

### 3.4. *Influence of contact time*

As shown in Fig. 7, the concentrations of Al and Si increase as the reaction proceeds until a maximum point, and decrease rapidly, or remain constant transiently, and start decreasing afterwards due to the precipitation and gelation of Al- and Si-containing species. Additionally, the possible formation of $Na_2O_3$–$Al_2O_3$–$SiO_2$–$H_2O$ (N-A-S-H) limits the further dissolution of the species as this gel covers the surface of the particles and works as a barrier [16,19]. The maximum dissolved concentration for Al at these conditions (12 M NaOH at 40 °C) were achieved in 12 h and 24 h for FA1 and FA2, respectively. Si concentrations in the solution at same conditions continued to increase until 12 h (FA1) and 72 h (FA2), followed by a sharp or gradual decrease due to the precipitation, which indicates that the dissolution behaviours of aluminosilicates change depending on the ash source.

The differences between the Al and Si dissolutions are also highlighted in Fig. 7, suggesting that these species have slightly different dissolution kinetics in concentrated NaOH solutions, [16,20,31]. The higher dissolution rate of Al in the early stages of the reaction may be explained by the preferential dissolution of Al from fly ash into the NaOH solution [29]. Furthermore, it is known that high $Al(OH)_4^-$ concentration in the reaction medium has an inhibiting influence on the dissolution of Si as it is responsible for the Al sorption onto the surface of the dissolving silanol particles when paired with the present alkali ions [30].

As the dissolution proceeds, the relative increase in the Si concentration is greater than that of Al, which can be seen as a continuous increase of Si/Al values for all biomass ash samples (see Figs. 3 and 4 above). These results corroborate the findings of a great deal of previous work on aluminosilicates dissolution in alkaline media [17,20,22,33]. According to the three-stage reaction mechanism suggested by Rees [34], in a geopolymerisation process, a high proportion of the glassy phase in the aluminosilicate source dissolves in stage 1 (dissolution stage). This is followed by the induction stage where an Al-rich metastable gel (Gel 1) is produced which forms a layer on the unreacted fly ash fraction. As the Al-rich aluminosilicate gel forms, the quantity of the detached Si increases which subsequently accelerates its dissolution. The third stage is called “the silicon incorporation stage” and here Gel 1 is transformed into Gel 2 which has higher Si concentrations [34]. It can therefore be assumed that the induction period takes place until 12 h (FA1) and 24 h (FA2), due to the decrease in Al concentrations in the solution.

As Fig. 7 shows, there is a significant difference between the dissolution kinetics of the aluminosilicates from FA1 and FA2. Reaction kinetics in this case depend on multiple variables such as pH of the alkali solution, type, and concentration of the alkali solution, contact time, temperature, composition, and the specific surface area of the solids. Other possible reasons for the different dissolution kinetics may be the processes the ashes went through after their collection, and the number of semi-amorphous cenospheres whose dissolution behaviour is different than that of the amorphous fraction [8]. As presented in Section 3.1, the specific surface area of FA2 is considerably smaller than that of FA1, which may have hindered the dissolution reaction. Furthermore, a strong relationship between the reactive aluminium content of the ash and the dissolution kinetics has been reported in the study of Fernández-Jiménez et al. [33], who found that the dissolution of Si is retarded in the absence of reactive Al. Therefore, the slower dissolution kinetics of FA2 might be attributed to its lower content of Al, as shown by the results of ICP-MS, EDS and XRF analyses.

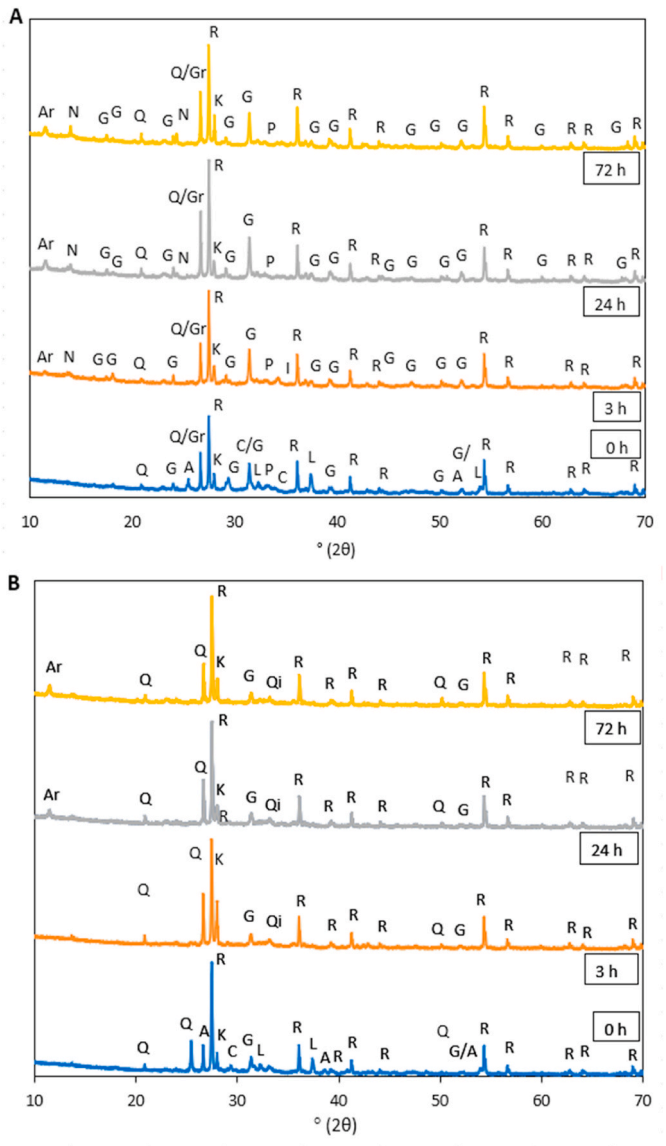


**Fig. 11.** XRD patterns of A: FA1, and B: FA2 with respect to the dissolution time; Peaks: A: anhydride, Ar: ardealite, C: calcite, G: gehlenite, G: graphite, I: imandrite, K: kyanite, L: lime, N: sodium aluminium silicate hydrate (N-A-S-H), P: portlandite, Q: quartz, R: rutile (standard).

### 3.5. Kinetic modelling

The kinetic modelling results for the dissolution of the biomass ashes are presented in Table 4, Fig. 8, and Fig. 9. The reaction rate of a non-catalytic heterogeneous solid-liquid system may be determined by diffusion through the layer of the reaction product, by diffusion through a liquid film surrounding the particles, or by a chemical reaction occurring at the particle surface [35]. In the case of the Al dissolution, the best fit was achieved with a Kabai model for FA1 and FA2, having coefficients of determination ($R^2$) of 0.97 and 0.98, respectively. The Kabai model describes the surface reaction as the rate-controlling step in the dissolution processes. The constants of average order were found to be 0.52 and 0.25 for FA1 and FA2, respectively, suggesting a deceleratory-shaped t-α curve. In addition to the Kabai model, the Valensi ($R^2 = 0.96$), Jander ($R^2 = 0.97$), and Ginstling-Brounsthein ($R^2 = 0.96$) models are suitable to describe the Al dissolution from FA1. The deceleratory nature of the Al dissolution can be seen in Fig. 7.

The best fit for the Si dissolution was achieved with 1-dimensional diffusion, Jander, Valensi and Ginstling-Brounsthein equations for FA1 and FA2. All four models have been frequently applied to investigate solid-liquid reaction systems [24,26,27], and propose a diffusion-controlled reaction where the reaction rate of the product is inversely correlated with the thickness of the layer occurring at the surface of the solid particles. Additionally, the Kabai, the shrinking disc model (SDM), and the shrinking core model (SCM) fit the experimental data of the Si dissolution from FA1 very well. Despite its frequent application in kinetics of the cementitious materials [36,37], the derivation of the Jander equation involves the neglection of the particle surface curvature. Therefore, the Jander equation is suitable in reactions with a reaction extent lower than 0.3.

### 3.6. Characterisation of the biomass fly ash dissolution residues

#### 3.6.1. XRD

The dissolution process was observed to have a slight influence on crystalline minerals present in the samples. Quantitative XRD results and X-Ray diffraction patterns of the biomass fly ash residues are shown in Fig. 10 and Fig. 11, respectively. The diffractograms are illustrated as a function of the dissolution time for the samples (before dissolution and after 3 h, 24 h and 72 h dissolution time). As explained previously (Section 2.1), rutile was utilised as the internal standard for the quantitative XRD analysis; therefore, its peaks will not be discussed. The relationship between the amorphous contents of biomass ashes and their dissolution behaviour was examined previously by Chaunsali et al. [22], and it was reported that the dissolved concentrations of Al and Si increase in addition to their faster dissolution kinetics from ashes with greater amorphous content. Nevertheless, in this study, the difference in the amorphous contents of the ashes falls in the statistical error range which limits to propose such a correlation.

According to Fig. 10A, the main crystalline phases in FA1 are quartz ($SiO_2$), calcite ($CaCO_3$), kyanite ($Al_2SiO_5$), anhydride ($CaSO_4$), gehlenite ($Ca_2Al_2SiO_7$), graphite, portlandite ($Ca(OH)_2$), qingheiite ($Na_2FeMgAl(PO_4)_3$), pigeonite (Ca,Mg,Fe) $(Mg,Fe)Si_2O_6$, sarcolite ($Na_4Ca_{12}Al_8Si_{12}O_{46}(SiO_4,PO_4)$ $(OH,H_2O)_4(CO_3,Cl)$), albite ($NaAlSi_3O_8$), and lime (CaO). Fig. 10A shows a diffractogram of the samples where some of these minerals can be recognised. One important finding was the substantial decrease and disappearance of the peaks of anhydride, lime, calcite and portlandite with increasing dissolution time. This may be due to their reaction with the hydroxides of the alkaline media and producing portlandite (3 h) which subsequently formed sodium aluminium silicate hydroxide hydrate (N-A-S-H) (72 h) by reacting with the alkali source and the aluminosilicates under the highly alkaline medium, as described by Alonso and Palomo [38]. In addition to the N-A-S-H, an ardealite ($Ca_2(HPO_4)(SO_4)H_2O$) peak is formed after 3 h of dissolution. According to Fig. 11A, the decrease in the amounts of kyanite and qingheiite is proportional to the dissolution time. Nevertheless, the concentrations of gehlenite and pigeonite increase in the early stages of the dissolution and start decreasing after 24 h. The concentrations of quartz, albite and graphite in the solid residue do not change significantly over time, it can thus be inferred that these phases do not react to a greater extent during the dissolution and remain relatively intact. The expected semi-amorphous halo around 20–30° (2θ) was observed to be very weak and slightly visible (72 h); therefore, it cannot be used for a precise quantification of the reactive phase in geopolymer precursors.

As shown in Fig. 10B, the crystalline phases in FA2 are quartz, anhydride, kyanite, gehlenite, calcite, qingheiite, anorthite ($Ca(Al_2Si_2O_8)$), albite, and lime. The solid residue obtained from the dissolution of FA2 showed no trace of semi-amorphous phase due to the absence of the semi-amorphous hump expected around 20–30° (2θ). The disappearance of the peaks representing anhydride (2θ = 26°), calcite (2θ = 29°), and lime (2θ = 37°) can be observed in Fig. 11B. This could have resulted from the reaction of these compounds with the hydroxides that produced, for example, ardealite (72 h). However, after a dissolution time of 3 h, no ardealite peak was formed, despite the disappearance of the three peaks representing lime, calcite, and anhydride. This may

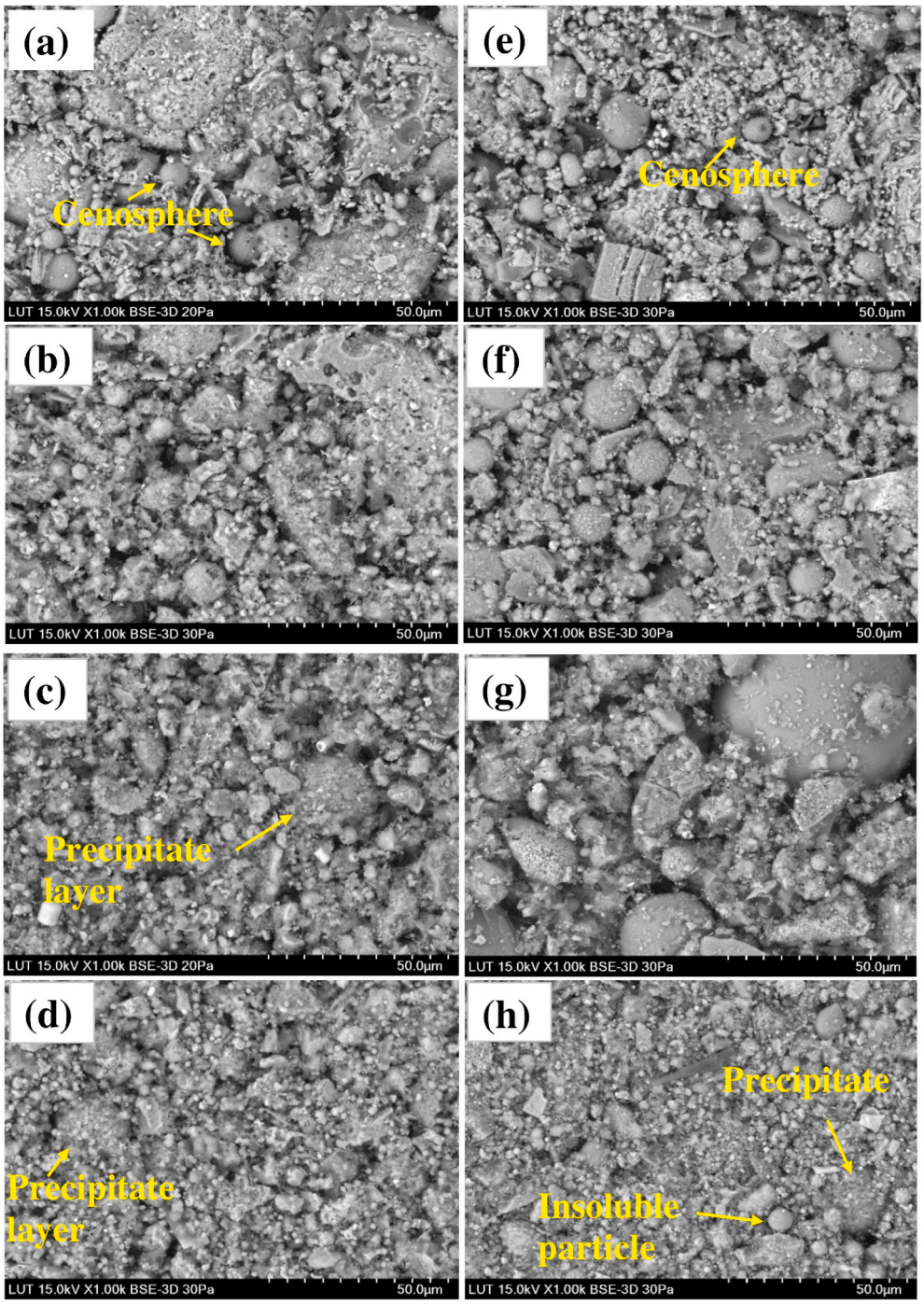


**Fig. 12.** SEM images of the biomass ash samples with respect to the dissolution time. Captions: a: before dissolution, b: 3 h dissolution, c: 24 h dissolution, and d: 72 h dissolution; FA2, e: before dissolution, f: 3 h dissolution, g: 24 h dissolution, h: 72 h dissolution.

indicate that the complete dissolution of lime, calcite and anhydride was achieved in 3 h. Different from FA1, no peak was observed representing the N-A-S-H compound at $2\theta = 14^{\circ}$. In addition to quartz and albite, no significant change was observed in gehlenite, kyanite and anorthite contents (see Fig. 10B above) independent of the dissolution time, which suggests that these phases are poorly soluble or insoluble in the applied reaction conditions.

### 3.6.2. SEM-EDS

The SEM images of the samples (before and after dissolution) are presented in Fig. 12. The spherical particles of biomass fly ash are called cenospheres which contain high concentrations of aluminosilicates. However, these cenospheres are partially reactive, and they dissolve partly in the highly alkaline solutions. The dissolution could be enhanced by increasing the temperature, the NaOH concentration, or the dissolution time [20]. Fig. 12 illustrates the dissolution of cenospheres in two ways: first, with a prolonged reaction, the amount of cenospheres starts to decrease which was observed after 24 h and 72 h for FA1 and FA2. It can thus be suggested that the partially reactive cenospheres in biomass fly ashes start to dissolve after the given reaction times. Second, a layer covering the surface of the solid residues can be observed (Fig. 12C, D, G, and H). This layer may have formed as a result of the aluminosilicates precipitation since it is more visible after 24 h, which corresponds to the decrease of concentrations of Al and Si (see

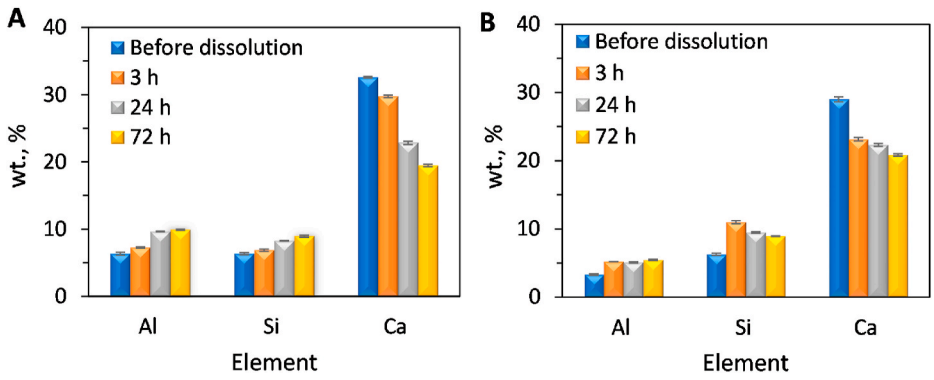


**Fig. 13.** EDS results of FA1 (A) and FA2 (B) showing the fractions of Al, Si and Ca.

Fig. 7 above). Data presented in the supplementary file (Fig. S1 – S8, EDS mappings) further confirms this suggestion where the Al and Si content could be seen locally agglomerated before the dissolution, whereas they are scattered on the entire surface of the materials after the dissolution (24 h onwards).

The EDS results of Al, Si and Ca in the dissolution residues are shown in Fig. 13. The increasing contents of Al and Si could be attributed to the dissolution of the larger Ca amount present in the ashes compared to that of Al and Si. These results further suggest that the dissolution of Ca occurred at a significantly higher yield compared to that of Al and Si, whose fractions seem to decrease as the reaction proceeds. This finding is also consistent with the XRD data, where the peaks of calcite, lime, and anhydride decrease and disappear with increasing dissolution times.

## 4. Conclusions

This work focused on defining the kinetics of Al and Si dissolutions from two different biomass-based fly ashes in NaOH solutions, using the NaOH concentration and temperature as the main variables. The findings of this study provide a new understanding of the release rates of aluminosilicates near equilibrium conditions from biomass-based fly ashes in alkaline solutions, which have a major impact on the properties of the geopolymerisation products. Based on the ICP-MS, XRF, quantitative XRD, and SEM-EDS analyses, the results of the study show that the dissolution kinetics of Al is faster compared to Si. The results also suggest that the dissolution yield of aluminium is significantly higher than that of silica, independent of the reaction conditions. Furthermore, it was shown that the NaOH concentration has a strong influence on the dissolution of Si, and that increasing the reaction temperature ($\leq$60 °C) not only accelerates the dissolution but also the reprecipitation. For the determination of the Si dissolution, it is suggested that a NaOH solution is applied with a minimum concentration of 9 M. The significantly different dissolution behaviour of aluminosilicates in FA1 and FA2 is likely to be related to the different specific surface areas of the biomass ashes, their different chemical compositions, and to their possibly different amorphous contents. In the comparison of the fourteen kinetic models, the dissolution of Al in NaOH solutions can be described very well with the Kabai model for both FA1 and FA2, whereas the 1-dimensional diffusion, Valensi, Jander, and Ginstling-Brounsthein models were found to be the most suitable to explain the dissolution kinetics of Si. The Rietveld analysis of the X-ray diffraction data demonstrated that quartz and albite are inert minerals in the ashes, while lime, anhydride and calcite are more readily soluble. Finally, although preliminary, this study suggests that these ashes may be utilised for the production of geopolymer composites. However, further research is required to investigate the viability of the precursors, since the characteristics of the composites cannot be predicted only by the dissolution behaviours.

## Declaration of competing interest

The authors declare that they have no known competing financial interests or personal relationships that could have appeared to influence the work reported in this paper.

## Acknowledgements

The authors would like to thank the European Regional Development Fund for their financial support through the Urban Innovative Actions Initiative [grant number UIA02-155]. The authors would like to acknowledge the contribution of Mr. Markus Riihimäki from Oulu University Analytical Services for the XRF analysis.

## Appendix A. Supplementary data

Supplementary data to this article can be found online at https://doi.org/10.1016/j.ceramint.2021.01.011.

## References

[1] USGS, Mineral Commodity Summaries, 2019, United States Geological Survey, Reston, Virginia, 2019, p. 204. https://prd-wret.s3-us-west-2.amazonaws.com/assets/palladiu m/production/atoms/files/mcs2019_all.pdf.
[2] Peter A. Claisse, Civil Engineering Materials, Butterworth-Heinemann, 2016, p. 160.
[3] European Commission, 2030 climate & energy framework. https://ec.europa.eu/cli ma/policies/strategies/2030_en#tab-0-0, 2014. (Accessed 17 September 2019).
[4] S. Lee, M. Seo, Y. Kim, H. Park, T. Kim, Y. Hwang, S. Cho, Unburned carbon removal effect on compressive strength development in a honeycomb briquette ash-based geopolymer, Int. J. Miner. Process. 97 (2010) 20–25, https://doi.org/10.1016/j.minpro.2010.07.0 07.
[5] H.S. Hassan, H.A. Abdel-Gawwad, S.R. Vásquez-García, I. Israde-Alcántara, N. Flores-Ramirez, J.L. Rico, M.S. Mohammed, Cleaner production of one-part white geopolymer cement using pre-treated wood biomass ash and diatomite, J. Clean. Prod. (2019) 1420–1428, https://doi.org/10.1016/j.jclepro.2018.11.137.
[6] M.A.M. Ariffin, M.A.R. Bhutta, M.W. Hussin, M. Mohd Tahir, N. Aziah, Sulfuric acid resistance of blended ash geopolymer concrete, Construct. Build. Mater. 43 (2013) 80–86, https://doi.org/10.1016/j.conbuildmat.2013.01.018.
[7] I. Ismail, S.A. Bernal, J.L. Provis, R. San Nicolas, D.G. Brice, A.R. Kilcullen, S. Hamdan, J.S. van Deventer, Influence of fly ash on the water and chloride permeability of alkali-activated slag mortars and concretes, Construct. Build. Mater. 48 (2013) 1187–1201, https://doi.org/10.1016/j.conbuildmat.2013.07.106.
[8] L.N. Assi, E.E. Deaver, P. Ziehl, Effect of source and particle size distribution on the mechanical and microstructural properties of fly Ash-Based geopolymer concrete, Construct. Build. Mater. 167 (2018) 372–380, https://doi.org/10.1016/j.conbuildmat.2018.01.193.
[9] P. Chindaprasirt, T. Chareerat, V. Sirivivatnanon, Workability and strength of coarse high calcium fly ash geopolymer, Cement Concr. Compos. 29 (2007) 224–229, https://doi.org/10.1016/j.cemconcomp.2006.11.002.
[10] J. Davidovits, Geopolymer Chemistry and Applications, fourth ed., Geopolymer Institute, Saint-Quentin, France, 2011.
[11] P. De Silva, K. Sagoe-Crenstil, V. Sirivivatnanon, Kinetics of geopolymerization: role of $Al_2O_3$ and $SiO_2$, Cement Concr. Res. 37 (2007) 512–518, https://doi.org/10.1016/j.cem conres.2007.01.003.

[12] A. Van Riessen, N. Chen-Tan, Beneficiation of Collie fly ash for synthesis of geopolymer: Part 1–Beneficiation, Fuel 106 (2013) 569–575, https://doi.org/10.1016/j.fuel.2012. 11.070.
[13] P. Chindaprasirt, C. Jaturapitakkul, W. Chalee, U. Rattanasak, Comparative study on the characteristics of fly ash and bottom ash geopolymers, Waste Manag. 29 (2009) 539–543, https://doi.org/10.1016/j.wasman.2008.06.023.
[14] C. Ma, A.Z. Awang, W. Omar, Structural and material performance of geopolymer concrete: a review, Construct. Build. Mater. 186 (2018) 90–102, https://doi.org/10.1016/j.conbuildm at.2018.07.111.
[15] S. Samantasinghar, S.P. Singh, Effect of synthesis parameters on compressive strength of fly ash-slag blended geopolymer, Construct. Build. Mater. 170 (2018) 225–234, https://doi.org/10.1016/j.conbuildmat.2018.03.026.
[16] N. Cristelo, P. Tavares, E. Lucas, T. Miranda, D. Oliveira, Quantitative and qualitative assessment of the amorphous phase of a Class F fly ash dissolved during alkali activation reactions - effect of mechanical activation, solution concentration and temperature, Compos. B Eng. (2016) 1–14, https://doi.org/10.1016/j.compositesb.2016.08.001.
[17] N. Granizo, A. Palomo, A. Fernandez-Jiménez, Effect of temperature and alkaline concentration on metakaolin leaching kinetics, Ceram. Int. 40 (2014) 8975–8985, https://doi.org/10.1016/j.ceramint.2014.02.071.
[18] J.J. Mazer, J.V. Walther, Dissolution kinetics of silica glass as a function of pH between 40 and 85 °C, J. Non-Cryst. Solids 170 (1994) 32–45, https://doi.org/10.1016/0022-3093(94)90100-7.
[19] K.U.A. Sanalkumar, M. Lahoti, E. Yang, Investigating the potential reactivity of fly ash for geopolymerization, Construct. Build. Mater. (2019) 283–291, https://doi.org/10.1016/j.c onbu.2019.07. 140.
[20] C. Kuenzel, N. Ranjbar, Dissolution mechanism of fly ash to quantify the reactive aluminosilicates in geopolymerisation, Resour. Conserv. Recycl. (2019), 104421, https://doi.org/10.1016/j.resconrec.2019.104421.
[21] C. Panagiotopoulou, E. Kontori, T. Perraki, G. Kakali, Dissolution of aluminosilicate minerals and by-products in alkaline media, J. Mater. Sci. 9 (2007) 2967–2973, https://doi.org/10.1007/s10853-006-0531-8.
[22] P. Chaunsali, H. Uvegi, R. Osmundsen, M. Laracy, T. Poinot, J. Ochsendorf, E. Olivetti, Mineralogical and microstructural characterization of biomass ash binder, Cement Concr. Compos. 89 (2018) 41–51, https://doi.org/10.1016/j.cemconcomp.2018.02.011.
[23] H. Uvegi, P. Chaunsali, B. Traynor, E. Olivetti, Reactivity of industrial wastes as measured through ICP-OES: a case study on siliceous Indian biomass ash, J. Am. Ceram. Soc. 102 (2019) 7678–7688, https://doi.org/10.1111/jace.16628.
[24] W.E. Brown, D. Dollimore, A. Galwey, Comprehensive Chemical Kinetics, CH Bamford and CFH Tipper, 1980.
[25] J. Kabai, Determination of specific activation energies of metal oxides and metal oxide hydrates by measurement of the rate of dissolution, Acta Chim. Acad. Sci. Hungar. 78 (1973) 57–73.
[26] R. Salmimies, M. Mannila, J. Kallas, A. Häkkinen, Acidic dissolution of hematite: kinetic and thermodynamic investigations with oxalic acid, Int. J. Miner. Process. 110 (2012) 121–125, https://doi.org/10.1016/j.minpro.2012.04.001.
[27] J.E. House, Principles of Chemical Kinetics, second ed., Elsevier, United States of America, 2007.
[28] R.P. Girón, B. Ruiz, E. Fuente, R.R. Gil, I. Suárez-Ruiz, Properties of fly ash from forest biomass combustion, Fuel (2013) 71–77, https://doi.org/10.1016/j.fuel.2012.04.042.
[29] A. Hajimohammadi, J.S. van Deventer, Dissolution behaviour of source materials for synthesis of geopolymer binders: a kinetic approach, Int. J. Miner. Process. (2016) 80–86, https://doi.org/10.1016/j.minpro.2016.05.014.
[30] B.R. Bickmore, K.L. Nagy, A.K. Gray, A.R. Brinkerhoff, The effect of Al (OH)$^{-}$ on the dissolution rate of quartz, Geochem. Cosmochim. Acta 70 (2006) 290–305, https://doi.org/10.1016/j.gca.2005.09.017.
[31] I. Nikolić, A. Drinčić, D. Djurović, L. Karanović, V.V. Radmilović, V.R. Radmilović, Kinetics of electric arc furnace slag leaching in alkaline solutions, Construct. Build. Mater. (2016) 1–9, https://doi.org/10.1016/j.conbuildmat.2016.01.038.
[32] S. Wang, L. Baxter, Comprehensive study of biomass fly ash in concrete: strength, microscopy, kinetics and durability, Fuel Process. Technol. 88 (2007) 1165–1170, https://doi.org/10.1016/j.fuproc.2007.06.016.
[33] A. Fernández-Jiménez, A. Palomo, I. Sobrados, J. Sanz, The role played by the reactive alumina content in the alkaline activation of fly ashes, Microporous Mesoporous Mater. 1 (2006) 111–119, https://doi.org/10.1016/j.micromeso.2005.11.015.
[34] C. Rees, Mechanisms, and Kinetics of Gel Formation in Geopolymers, The University of Melbourne, 2007.
[35] O. Levenspiel, Chemical Reaction Engineering, third ed., John Wiley & Sons, USA, 1999.
[36] C. Chen, W. Gong, W. Lutze, I.L. Pegg, J. Zhai, Kinetics of fly ash leaching in strongly alkaline solutions, J. Mater. Sci. 3 (2011) 590–597, https://doi.org/10.1007/s10853-010-49.97-z.
[37] Z. Hu, M. Wyrzykowski, P. Lura, Estimation of reaction kinetics of geopolymers at early ages, Cement Concr. Res. (2020), 105971, https://doi.org/10.1016/j.cemconres.2020.105971.
[38] S. Alonso, A. Palomo, Calorimetric study of alkaline activation of calcium hydroxide–metakaolin solid mixtures, Cement Concr. Res. 1 (2001) 25–30, https://doi.org/10.1016/S0008-8846(00)00435-X.